Model Predictive Control with On-line Kinetic Parameter Identification Strategy on Anaerobic Digestion Reactors

Luis G. Cortés [1,†,‡] (ID), **Julio Barbancho** [1], **María A. de la Rubia** [2], **Diego F. Larios** [1], **Jose D. Marín** [2], **A.F. Mohedano** [2], **Christian Portilla** [3]

[1]   Department of Electronic Technology, Polytechnic School, University of Seville; luicoroca@alum.us.es
[2]   Chemical Engineering Department, Universidad Autonoma de Madrid, Campus de Cantoblanco, 28049, Madrid, Spain; angeles.delarubia@uam.es
[3]   Facultad de Minas, Universidad Nacional de Colombia, Robledo, 050034, Medellín, Antioquia; crportil@unal.edu.co
*   Correspondence: luicoroca@alum.us.es; Tel.: +34 656957248 (Spain)
†   Escuela Politécnica Superior de la Universidad de Sevilla, Calle Virgen de África, 7, 41011 Seville, Spain
‡   These authors contributed equally to this work.

Abstract: This work presents a nonlinear model predictive control scheme that challenges overcoming the obstacles holding back over decades to develop affordable autonomous control and monitoring systems applied in the large-scale industry. Among the numerous proposals in the literature, most do not consider the significant fluctuation of kinetic parameters in the reduced mathematical model ADM2, widely used for control and monitoring purposes. The prevalent cause, on a basis, is the lack of information caused by some dynamics and parameters that cannot be measured in real-time by reliable sensors. In addition, to make matters worse, those systems inherently act with nonlinear nature and have a high sensitiveness to uncontrollable inputs and perturbations. Therefore, to prevent these drawbacks, this work proposes a new methodology that reconstructs the lack of information from the non-measurable dynamics, concentration of bacterias, and the kinetic parameters related to reaction rates. Simulations results demonstrate the effectiveness of the methodology compared with traditional industrial control schemes.

Keywords: model predictive control; asymptotically observer; kinetic parameter observer; homoge-neous reaction systems; anaerobic digestion

1. Introduction

Anaerobic digestion (AD) treatment reactors are not a very common technology widespread at industrial scale, and less than usual even find control and monitoring schemes operating those systems. The AD process has attractive advantages in comparison to classical alternatives like aerobic digestion systems or composting; it returns little sludges, has a positive overall energy balance, and also has an enormous potential to reduce challenging and concentrated substrates such as animal wastes, wastewater, by-products from industrial plants, and food wastes to name the most important ones. However, to move forward aiming to evolve to autonomous control and monitoring system, too many obstacles have to be overcome, like the inherent problems of acting with nonlinearities. Additionally, essential singularities as high sensitiveness to uncontrollable inputs and perturbations, and the drawbacks caused by the restricted access to online measurements due to the lack of the existence of cost-efficient and reliable sensors, originate mathematical models with limited approximation to real data. To start solving these drawbacks, this paper proposes a substitution of the physical sensors for software online transducers in order to access reliable data, carrying out an estimation based on the available measurements over the reaction system [1,2].
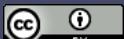
Thus, a necessary condition must be satisfied when reliable control and monitoring algorithms must be designed. The information obtained from anaerobic reactors need to be sensed in real time with reliable instruments or methods in order to feed mathematical models, and so, to follow the evolution of reactions, and ensure early detection of faults. Then, it is necessary to guarantee a continuous flow of data on demand. The key variables of the reaction system, the concentrations of biomass, substrate, and metabolite, as well as the kinetics of reactions, are measured by laboratory procedures. However, the drawbacks related to this process are the high operational costs and the high time lapsed between measurements and results. Hence, the design of software sensors allowing regular communication between reality and the data needed by the algorithm is one of the main concerns of this paper. The ADM2 model with modifications in some dynamics (to enable a broad spectrum of usable types of organic matters at influent) is the mathematical model selected to represent the system [3]. Specifically, the model has two inconveniences. Two dynamics are impossible to measure directly; first, the data coming from acidogenic and methanogenic bacterias concentrations, and second, the data from the kinetic yield parameters. Due to the importance of accurate knowledge of data from the system, specific observers were proposed due to the bacterias considered are high sensitiveness to weak changes in the reaction system [4,5].

Because the AD processes are related to the existence of microorganisms, the phenomenology is frequently poorly comprehended. Replicating the same operation conditions is not possible regularly due to the uncertainty and variation in the yield parameters since the metabolisms vary. This paper aims to contribute with new software that also looks beyond the traditional methods, where the performance depends on measured data and new software sensors strategies that enable a step forward to capture the reality with better reliability. In order to perform a long-term strategical plan to achieve feasible control schemes for industrial purposes, the first step is to ensure the availability of the measure layer, providing the mathematical model with required data. Based on information found in literature, the use of state observers has emerged in the last decades as one of the most common alternatives because of its relatively easy use. High gain observers, Kalman and extended Kalman filters, asymptotic observers, and the estimation of reaction rates are the most commonly used in bioprocess. However, there is no evidence in literature designing observer structures related to estimating dynamics and kinetic parameters in the anaerobic digestion process. Pross in-depth knowledge of the process kinetics is an extreme challenge in numerous engineering applications; therefore, there is a huge motivation to search for a category of observers which allows one to asymptotically reconstruct the missing states even when the kinetics are unknown. A cascade structure of an asymptotic observer to estimate the concentration of acidogens and methanogens is proposed followed by a kinetic parameters observer that estimates two reaction rates of the process [6–8].

Monitor and control schemes are essential to achieve an adequate operation in anaerobic digestion reactors. Among the alternatives registered on literature, the model predictive control (MPC) have several benefits compared with traditional methods [1,9,10]. This algorithm uses a mathematical model to make predictions to see the evolution of the system in advance, then an optimization algorithm calculate the correspondent control actions. One of the main advantages is that it is possible to explicitly program the physical and operations constraints controller have physical and operational constraints, allowing to work under feasible operational conditions. However, one of the main obstacles are the nonlinearities, thus, the control strategies based on mathematical models have to be nonlinear too. On literature we find a diverse type of those systems, such as nonlinear PID, sliding mode control, parametrized nonlinear MPC, and game theory nonlinear MPC to name some examples. In general, although those control schemes have shown an affordable performance, the implementation is the main drawback, specially if the system is subjected

to constraints [11–13].

This paper is organized as follows. Section 2 explains the mathematical anaerobic digestion model ADM2, used for control purposes, proposed with additional terms to include a wide spectrum of organic matter in operation. Then, section 3 shows the parameter identification procedure based on optimization that adjusts the model ADM2 to experimental data and the hierarchical observer structure proposed, which unlocks the possibility of being aware of the lack of information due to the absence of reliable sensors. In section 4, the controller MPC structure proposed is explained. Finally, section 5 shows the results of the improvements achieved by using the MPC controller compared with other similar structures and traditional solutions found in the industry like the PID controllers.

2. Mathematical modeling and experimental data

2.1. Mass-Balance Mathematical Model for Anaerobic Digestion reactors

The mathematical model used to represent the anaerobic digestion process inside a reactor is presented as follows. The new version of the model ADM2, proposed by Luis Cortés et al. [14], comes from the need to develop an appropriate methodology to design control and monitoring systems that consider a wide spectrum of organic matters. Therefore, the new equation system is shown as follows.

$$\frac{dX_1}{dt} = X_1(\mu_1 - \alpha D), \tag{1}$$

$$\frac{dX_2}{dt} = X_2(\mu_2 - \alpha D), \tag{2}$$

$$\frac{dS_1}{dt} = D(S_{1_{in}} - S_1) - \psi_1\left(\frac{S_1}{K_{S1} + S_1}\right), \tag{3}$$

$$\frac{dS_2}{dt} = D(S_{2_{in}} - S_2) + k_{s_2,1}\psi_1\left(\frac{S_1}{K_{S1} + S_1}\right) - \psi_2\left(\frac{S_2}{K_{S2} + S_2}\right), \tag{4}$$

$$\frac{dZ}{dt} = D(Z_{in} - Z) + k_{Z,1}\psi_1\left(\frac{S_1}{K_{S1} + S_1}\right) + k_{Z,2}\psi_2\left(\frac{S_2}{K_{S2} + S_2}\right), \tag{5}$$

$$\frac{dC}{dt} = D(C_{in} - C) - q_C + k_4\mu_1 X_1 + k_5\mu_2 X_2, \tag{6}$$

with:

$$q_C = k_L a[C + S_2 - Z - K_H P_C] \tag{7}$$

where P_C and Φ comes from the equations described in Bernard et al. [15].

$$P_C = \frac{\Phi - \sqrt{\Phi^2 - 4K_H P_T(C + S_2 - Z)}}{2K_H} \tag{8}$$

with:

$$\Phi = C + S_2 - Z + K_H P_T + \frac{k_6}{k_L a}\mu_2 X_2 \tag{9}$$

X_1 represents the concentration of acidogenic bacterias, X_2 is the concentration of methanogenic archaeas, S_1 is the concentration of organic substrate, S_2 is the concentration of VFA, Z is the total alkalinity, and C is the concentration of inorganic carbon. The subscript "in" indicates influent flow correspondent to the concentrations S_1, S_2, C, and Z. D is the dilution rate. The yield coefficients k_1, k_2, k_3, k_4, k_5 and k_6 mean the yield for COD degradation, the yield for VFA production, the yield for VFA consumption, the yield for CO_2 production, the yield for CO_2 production, and the yield for CH_4 production respectively. The ammonium contribution to the alkalinity is considered in the mass-balance mathematical model

proposed by Kil et al. [13]. The following Monod-type representations characterize the 115
reaction rates $_1$ and $_2$: 116

$$\rho_1 = \psi_1 \frac{S_1}{K_{S_1} + S_1} \qquad (10)$$

and. 117

$$\rho_1 = \psi_1 \frac{S_1}{K_{S_1} + S_1}. \qquad (11)$$

Where ψ_1, ψ_2, K_{S1}, and K_{S2} describe the maximum rate of acidogenic degradation, the 118
maximum rates of methanogenic degradation, the half-saturation constant associated with 119
substrate S_1, and the half-saturation constant associated with the substrate S_2 respectively. 120
Monod-type kinetics describe the growth of acidogenic bacteria ψ_1 (S_1) and methanogenic 121
archaea ψ_2 (S_2) because, in the fermentation process, the biomass does not register possible 122
VFA accumulation and consequently inhibition. Finally, the methane flow rate produced 123
q_M is proportional to the reaction rate of methanogenesis, as shown in the following 124
equation: 125

$$q_M = k_{CH_4} \psi_2 \left(\frac{S_2}{K_{S2} + S_2} \right) \qquad (12)$$

2.2. Experimental Data from the Pilot Plant Anaerobic Digester 126

The data set in this paper were collected from a CSTR pilot plant (150 L) that operates at 55 127
± 2 °C (thermophilic range). The experiment occurred in Guadalete (Jerez de la Frontera, 128
Spain) on a sewage treatment plant []. The system operates with diary inlet flow with 129
primary and secondary combined waste sludges. The study was conducted to test the 130
effects of step changes in the solid retention time (SRT) during 338 days. The experiment 131
started at SRT in 75 days. It gradually decreases to steps 40 days, 27 days, 20 days, and 15 132
days (see details on Table 1). However, for modeling purposes, only a specific range of data 133
was used to discard unstable scenarios, which are unfavorable for modeling purposes due 134
to deviations from the natural behavior of reactions. Thus, 207 days were selected, aiming 135
to work with standard patterns of microorganisms as much as possible. 136

Table 1. OLR stages during the 338 days experiment.

SRT	Days	
	Start	End
75	1	45
40	46	85
27	86	170
20	171	253
15	254	323

The data selected starts at SRT in 40 days, the organic loading rate (OLR) equivalent was 137
0.8 $KgVS/m^3day$ (or 1.5 $KgCOD/m^3 day$). This value remains constant until a steady state 138
is reached; that is when the measurements of VS and COD removals and the production 139
rate of CH_4 are the means of the latest measurements. The first change in the value of SRT 140
occurred on the day 40 from the data selected, where the SRT switched to 27 days. At this 141
new stage, the system operates from the day 40 until the day 124. Finally, at the day 125, the 142
SRT value decreases to 20 days. This stage took place on the day 124. This value remained 143
constant until the end of the experiment, the day at 208. Only in specific situations, when 144
the value of pH decreased beyond 7.3, a small amount of sodium carbonate was added at a 145
concentration of 2N to keep the value of pH over a feasible operational range. 146

147

Figure 1 is shown some of the data used to describe the status of the anaerobic digestion process inside the reactor. The information shown was used to perform an identification procedure to characterize the mathematical model and adjust the experimental data. The Figure 1a, Figure 1b, Figure 1c, and Figure 1d are the chemical oxygen demand (COD) at influent, the volatile fatty acids (VFA) at influent, the volatile fatty acids (VFA) on effluent, and the volume of CH_4 produced respectively.

3. Parameter identification and on-line measurements

Consider the non-linear anaerobic digestion mathematical model from equations (1) to (6). The parameter identification algorithm, that calculates the optimal parameters $p(k)$ (see Figure 2a), uses the information coming from three sources. $F_{out} = \{CH_4\}$, the volume of methane produced as a consequence of the metabolism by arquea methanogenic. $n_m = \{S_1, S_2, Z\}$, the measured states considered by the model ADM2, the organic substrate concentration, the volatile fatty acids concentration, and the total alkalinity. Finally, the level of pH. $n_{nm} = \{X_1, X_2, C\}$ are the non measured data. The vector $u_{out} = \{n_{nm}, n_m, pH\}$ are the variables on the effluent. Finally, Q_{in} represents the energy from an external source delivered to the reaction inside the reactor. Table 2 list the parameters identified by the method proposed (to check more details see [14]). This method solves an optimization problem to find the values of parameters aiming to minimize the difference between the measured data from the experiment and the correspondent variables on the model ADM2 modified [6].
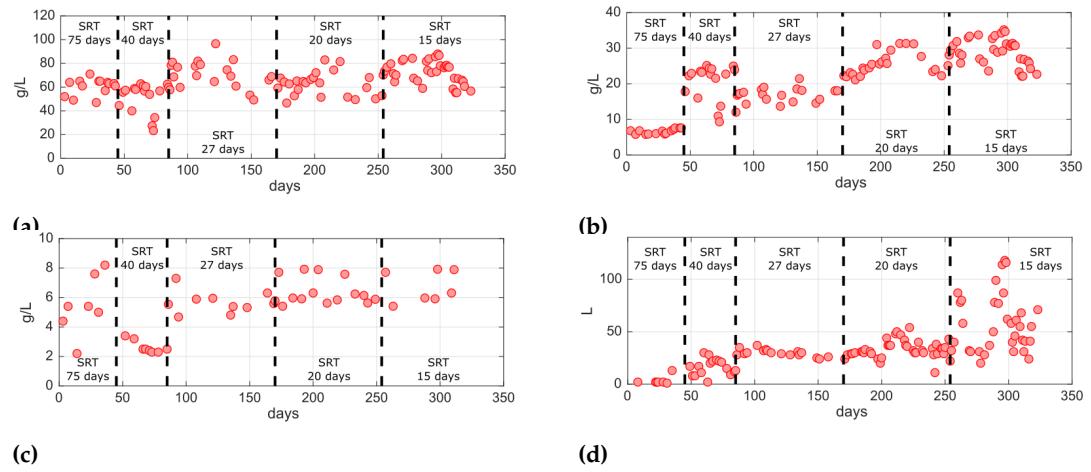
Figure 1. Influent measurements. (**a**) chemical oxygen demand (COD); (**b**) volatile fatty acids (VFA). (**c**) Volatile fatty acids (VFA) at effluent. (**d**) Volumen of CH_4 produced.

The equation (13) shown the optimization problem proposed to be solved.

$$\min_{p(k),...,p(k+N_F)} J(p(k), y(k))$$

s.t.

$$
\begin{aligned}
&x(k+1) = f(x(k), p(k)), \\
&y(k) = g(x(k), u(k)), \\
&y_{min} \leqslant y(k) \leqslant y_{max}, \forall k = 1, ..., N_p, \\
&p_{min}, \leqslant u(k) \leqslant p_{max}, \forall k = 1, ..., N_u
\end{aligned}
\tag{13}
$$

The function $J(u(k), y(k))$ represents the function to be minimized, depending on the optimal parameters $p(k)$, the output $y(k)$, and the state dynamics $x(k)$. y_{min} and y_{max} are the lower and upper operational boundaries. p_{min} and p_{max} are the lower and upper

boundaries of the optimal parameters calculated. Thus, the variables to be calculated are $p(k) \in \{\mu_{1max}, K_{SI}, \mu_{2max}, K_{S2}, k_1, k_2, k_3, k_4, k_5, k_6, K_{Z_1}, K_{Z_2}, Z_{in}\}$.

$$J(u(k), y(k)) = norm\left((x_{mod}(k) - x_e)^2\right) \tag{14}$$

In the previous equation, it is observed that the proposed function is the norm of the difference squared between the measured $x_e(k)$ and the correspondent data from the model $x_{mod}(k)$.

Table 2. Parameters identified on the optimization algorithm.

Parameter	Description	Value	Unit
μ_{1max}	Maximum acidogenic bacteria growth rate	0.06	d^{-1}
μ_{2max}	Maximum metanogenic bacteria growth rate	0.05	d^{-1}
K_{S_1}	Half saturation constant	298.03	g/L
K_{S_2}	Half saturation constant	1.08	$mmol/L$
k_1	Yield for substrate degradation	1.34×10^{-6}	[]
k_2	Yield for VFA production	216.80	$mmol/g$
k_3	Yield for VFA consumption	14.23	$mmol/g$
k_4	Yield for CO_2 production	8.58×10^{-7}	$mmol/g$
k_5	Yield for CO_2 production	1.14×10^{-6}	$mmol/g$
k_6	Yield for CH_4 production	550.00	$mmol/g$
K_{Z_1}	Yield for aminoacids degradation	3.21	$mmol/L$
K_{Z_2}	Yield for proteins degradation	4.45	$mmol/L$
Z_{in}	Total alkalinity at inlet	19.66	$mmol/L$

Thus, the equation below shows the details of the proposed function.

$$J(n_m(k), u(k)) = norm\left(\left(n_m^{mod}(k) - n_m^e(k)\right)^2 + \right.$$
$$\left.\left(pH^{mod}(k) - pH^e(k)\right)^2 + \left(q_M^{mod}(k) - q_M^e(k)\right)^2\right) \tag{15}$$

The aforementioned equation represents the mean square error between the experimental data; $(n_m^e(k), pH^e(k)$ and $q_M^e(k))$, and the correspondent data from the model; $(n_m^{mod}(k), pH^{mod}(k)$ y $q_M^{mod}(k))$. The parameters to be adjusted are exposed on the following vector $u(k) = \{\mu_{1max}, K_{SI}, \mu_{2max}, K_{S2}, k_1, k_2, k_3, k_4, k_5, k_6, K_{Z_1}, K_{Z_2}, Z_{in}\}$.

(a)   **(b)**
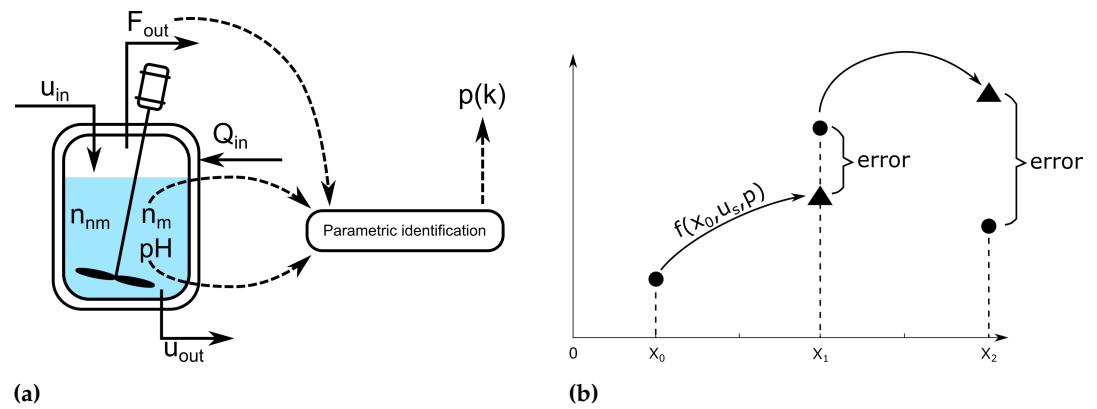
Figure 2. Optimal-based schematics procedures. (**a**) identification parametric diagram; (**b**) s ahead algorithm.

3.1. Parameter identification using pattern search by step-ahead

Figure 2b shows the step-by-step structure of the algorithm to estimate the parameters. The technique, called step-ahead, uses the mathematical model as the core to predict the evolution of the system's dynamics. Consider X_0 as the starting point (represented by a black circle ●). At this point, using the inputs, the control actions, and the measurements of the system, the algorithm uses the mathematical model to calculate the next step in advance, aiming to discover the system's evolution (represented by a black triangle ▲). In the next step, in X_1, the prediction (the ▲) is compared with the value measured (the ●). The previous operation completed on each step along the experiment is the error on each step accomplished by the method. Finally, all this information is stored on the vector as follows.

$$E = [error_1, error_2, ..., error_n] \tag{16}$$

Where n represents the total number of days of the experiment. The optimization problem is shown in the following equations.

$$\min_{u(k)} E \tag{17}$$

$$\text{s.t.}$$

$$n_m(k+1) = f(n_m(k), u(k)),$$
$$n_{nm}(k+1) = f(n_{nm}(k), u(k)),$$
$$0 \leqslant u(k) \leqslant p_{max}, \forall k = 1, ..., t_f$$

$$\tag{18}$$

Figure 3 shows the results of the adjustment made by the parametric optimization algorithm. Figure 3a and Figure show the results of VFA and COD; the data measurements from the reactor (red line) and the adjustment achieved by the parameters calculated and used by the model. The results were excellent.

(a)   **(b)**
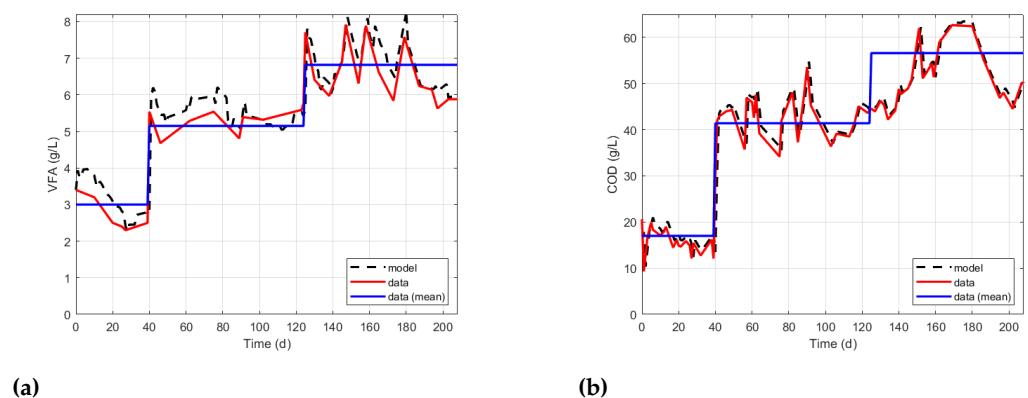
Figure 3. Mathematical model adjustment to experimental data in the step-ahead algorithm. (**a**) Volatile fatty acids (VFA), variable S_2. (**b**) Chemical oxigen demand (COD), variable S_1.

3.2. Asymptotic Estimator

There is one significant problem using control and monitoring systems in anaerobic digestion reactors; it is not yet possible to achieve all measurements online to feed the mathematical model and run the controller. The absence of information due to the lack of reliable sensors and the inadequate strategies to test constant measurements through laboratory analyses opens up an opportunity to substitute the uncertainty by the design of software sensors. This technology estimates the state variables, and concentrations of

acidogenic and methanogenic bacterias, without the information of the reaction kinetics in stoichiometric equations. It results in a particular category of observers named asymptoti- cally, where two conditions support the estimation of the non-measurable dynamic states; the system is still not exponentially observable, and the reaction kinetics are unknown. The following conditions influence the design of the algorithm: the information of the matrix ϕ is unknown, the yield coefficients from K are fully known, and the number of q_{state}, the number of measured state variables is the same or higher than the rank of the matrix K (that is $q_{state} = dim(\xi_1) \geq= rank(K)$). Hence, consider the general equation of homogeneous reaction systems described by a general nonlinear state space model.

$$\frac{d\xi}{dt} = K\phi(\xi, t) - D\xi - Q(\xi) + F. \tag{19}$$

where $dim(\xi) = dim(F) = dim(Q) = N$, $dim(\phi) = M$ y $dim(K) = N \times M$. Thus, the general nonlinear model equation (19) can be divided as.

$$\frac{d\xi_a}{dt} = K_a\phi(\xi_a, \xi_b) - D\xi_a - Q_a + F_a, \tag{20}$$

$$\frac{d\xi_b}{dt} = K_b\phi(\xi_a, \xi_b) - D\xi_b - Q_b + F_b, \tag{21}$$

Where the rank of K is p. The submatrix K_a results from a section of K with $p \times M$. The submatrix K_b has the remaining information of K. Finally, the matrices (ξ_a, ξ_b), (Q_a, Q_b) and (F_a, F_b) are the corresponding parts of ξ, Q and F caused by the influence of K_a and K_b. The previous formulation has the following feature. There exists a transformation that considers Z_{ob} as a linear combination of X_a and X_b, thus.

$$Z_{ob} = A_0\xi_a + \xi_b. \tag{22}$$

derived from the previous equation.

$$\dot{Z}_{ob} = A_0\dot{\xi}_a + \dot{\xi}_b. \tag{23}$$

then, using the equation (20) on the equation (23):

$$\dot{Z}_{ob} = A_0(K_a\phi - DX_a - Q_a + F_a) + K_b\phi - DX_b - Q_b + F_b. \tag{24}$$

solving the last equation.

$$\dot{Z}_{ob} = A_0K_a\phi - A_0DX_a - A_0Q_a + A_0F_a + K_b\phi - DX_b - Q_b + F_b, \tag{25}$$

then grouping the expressions.

$$\dot{Z}_{ob} = -D(A_0X_a + X_b) + A_0(F_a - Q_a) + F_b - Q_b + A_0K_a\phi + K_b\phi. \tag{26}$$

finally, using the equation (23) on equation (26), then:

$$\dot{Z}_{ob} = -DZ_{ob} + A_0(F_a - Q_a) + F_b - Q_b + \underbrace{\phi(A_0K_a + K_b)}_{eliminate}. \tag{27}$$

Two conditions remove the expression in (27). However $\phi \neq 0$, thus.

$$A_0K_a + K_b = 0, \tag{28}$$

Finally, according to the previous equations, the state space model is equivalent to.

$$\frac{d\xi_a}{dt} = K_a\phi(\xi_a, \xi_b) - D\xi_a - Q_a + F_a, \tag{29}$$

$$\frac{dZ_{ob}}{dt} = -DZ_{ob} + A_0(F_a - Q_a) + (F_b - Q_b). \tag{30}$$

The expression $F_a - Q_a = 0$ means the partition made by the equations (20) and (21) are appropriate due to the new dynamics on $_{ob}Z$ are independent from K and ϕ. On the equation (29) is shown $\check{\xi}_a$ is independent from ϕ (the information of the reaction kinetics).

Observer design

Using the nonlinear general dynamical model, equations (1) to (6), the following equations describes the decoupled subsystem conducted by the state variables X_1, X_2, S_1 and S_2 can be run separately. This representation allows working with a reduced model that can be written as.

$$\xi = \begin{bmatrix} X_1 \\ X_2 \\ S_1 \\ S_2 \end{bmatrix}, \quad F = \begin{bmatrix} 0 \\ 0 \\ DS_{1in} \\ DS_{2in} \end{bmatrix}, \quad Q = \begin{bmatrix} 0 \\ 0 \\ 0 \\ 0 \end{bmatrix}, \quad K = \begin{bmatrix} 1 & 0 \\ 0 & 1 \\ -k_1 & 0 \\ k_2 & -K_3 \end{bmatrix}, \quad \phi = \begin{bmatrix} \mu_1 X_1 \\ \mu_2 X_2 \end{bmatrix}. \tag{31}$$

Considering the previous subsystem, the subsequent state equation is structured as follows.

$$\frac{d}{dt}\begin{bmatrix} X_1 \\ X_2 \\ S_1 \\ S_2 \end{bmatrix} = \begin{bmatrix} 1 & 0 \\ 0 & 1 \\ -k_1 & 0 \\ k_2 & -K_3 \end{bmatrix}\begin{bmatrix} \phi_1 \\ \phi_2 \end{bmatrix} - D\begin{bmatrix} X_1 \\ X_2 \\ S_1 \\ S_2 \end{bmatrix} + \begin{bmatrix} 0 \\ 0 \\ DS_{1in} \\ DS_{2in} \end{bmatrix}. \tag{32}$$

Then, comparing the previous subsystem with the equivalent generic equations (29) and (30) results in the following conditions.

- The main nonlinear state space system is decoupled into two sections; the subsystem equation in (32), and the other one that includes the dynamics of inorganic carbon C and total alkalinity Z.
- The information contained on matrices Q_a and Q_b is located in the dynamic of C.
- Matrices Q_1 and Q_2 are the reaction rates r_1 and r_2.

Based on the previous information, ξ_a and ξ_b represents the measurable and no measurable states, thus.

$$\xi_a = \begin{bmatrix} S_1 \\ S_2 \end{bmatrix}, \quad \xi_b = \begin{bmatrix} X_1 \\ X_2 \end{bmatrix} \tag{33}$$

therefore.

$$Z_{ob} = \begin{bmatrix} Z_{ob_1} \\ Z_{ob_2} \end{bmatrix} = \begin{bmatrix} A_0\xi_a + \xi_b \end{bmatrix} = \begin{bmatrix} \frac{1}{K_1} & 0 \\ \frac{K_2}{K_1K_3} & \frac{1}{K_3} \end{bmatrix}\begin{bmatrix} S_1 \\ S_2 \end{bmatrix} + \begin{bmatrix} X_1 \\ X_2 \end{bmatrix} \tag{34}$$

using $Z = A_1\xi_1 + A_2\xi_2$ to compare with the previous structure in equation (34) results in.

$$A_2 = I \tag{35}$$

then, as a consequence, in order to find A_0.

$$A_0 = -K_bK_a^{-1} \tag{36}$$

Using the equation (36) and the information above, then it originates the following matrices.

$$K_b = \begin{bmatrix} 1 & 0 \\ 0 & 1 \end{bmatrix}, \quad K_a = \begin{bmatrix} -K_1 & 0 \\ K_2 & -K_3 \end{bmatrix}. \tag{37}$$

The next step is to separate the non-measurable states in order to estimate the variables Z_{ob_1} and Z_{ob_2}, and the measurable states S_1 and S_2. Using the equation (22) and solving for ξ_b.

$$\xi_b = Z_{ob} - A_0 \xi_a \tag{38}$$

At this point, we have the matrices of ξ_a, A_0 and Z_{ob}.

$$\xi_b = \begin{bmatrix} X_1 \\ X_2 \end{bmatrix}, \quad Z_{ob} = \begin{bmatrix} Z_{ob_1} \\ Z_{ob_2} \end{bmatrix}, \quad A_0 = \begin{bmatrix} \frac{1}{k_1} & 0 \\ \frac{k_2}{k_1 k_3} & \frac{1}{k_3} \end{bmatrix}, \quad \xi_b = \begin{bmatrix} S_1 \\ S_2 \end{bmatrix} \tag{39}$$

The states X_1 and X_2 are unknown, and Z_{ob_1} and Z_{ob_2} represent the new dynamics independent from the reaction kinetics contained on ϕ. The matrix A_0 has the yield coefficients, and the state variables S_1 and S_2 are the estimation space. Then, F_a and F_b are.

$$F_a = \begin{bmatrix} DS_{1in} \\ DS_{2in} \end{bmatrix}, \quad F_b = \begin{bmatrix} 0 \\ 0 \end{bmatrix} \tag{40}$$

Finally, using the previous equations, the expression of $\dot{Z}_{ob}$ is as follows.

$$\frac{dZ_{ob}}{dt} = -DZ_{ob} + A_0(Fa - Qa) + (F_b - Q_b) \tag{41}$$

3.3. Kinetic Parameter Reaction Estimator

This section presents an additional tool that complements the lack of measurements inside a reactor. The focus is to estimate the kinetic reactions coming from the reaction system. Figure 4 shows the structure proposed to achieve all information needed to feed the mathematical model on the control scheme strategy.
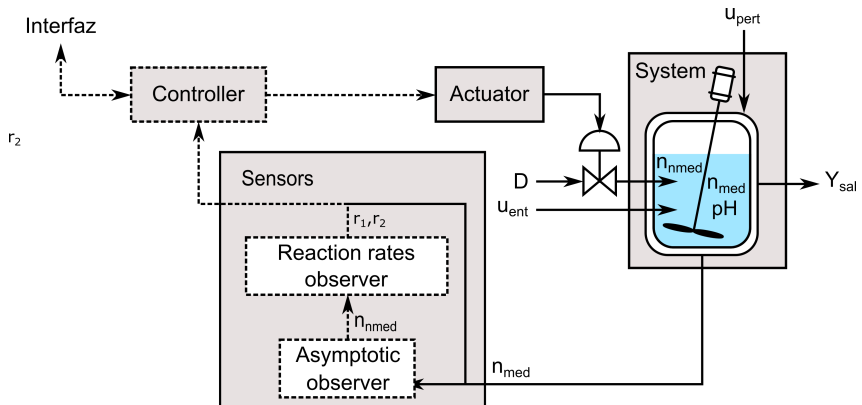
Figure 4. The structure proposed; an asymptotic observer and a kinetic parameter estimator on an anaerobic digestion reactor.

The discontinuous line represents the information generated by the observer algorithms making it possible to transfer the information needed to run the mathematical model. The discontinuous line ends with the information generated by the controller and delivered by the actuator. In order to design the kinetic estimator algorithm, considers the following nonlinear equation that represents the system.

$$\dot{\xi} = K\phi - D\phi - Q + F \tag{42}$$

The equation (42) assumes the coefficients from K are known, and the dilution rate D, the input flows F, and the gas output flows Q are measured in real-time. Additionally, it is assumed that ξ is fully-known because the un-measured dynamics are reconstructed by

the asymptotic observer designed in the previous section. The vector ϕ is partially known and is divided into two terms as follows.

$$\phi = H\rho, \tag{43}$$

The matrix H contains the information of the known kinetic reactions, and ρ contains the remaining information, the unknown kinetic reactions. Thus, using the equation (43) on (42) results on.

$$\dot{\xi} = KH\rho - D\phi - Q + F. \tag{44}$$

Thus, the estimation of reaction kinetics, r_1 and r_2, is equivalent to focus the estimation contained in ρ. Hence, the new dynamic system is presented as follows.

$$\dot{\hat{\xi}} = KH\hat{\rho} - D\xi - Q + F - \Omega(\xi - \hat{\xi}), \tag{45}$$

$$\dot{\hat{\rho}} = (KH)^T \Gamma(\xi - \hat{\xi}), \tag{46}$$

Where $\hat{\rho}$ represents the real-time estimation of ρ. The value of the equation 46, $\xi - \hat{\xi} = 0$, means that the system achieved the desired result. In contrast, the behaviour showed by the equation (45), when $\xi - \hat{\xi} = 0$ on equation (46) means that $\dot{\hat{\rho}} = 0$, resulting in a convergence to desirable reaction kinetics values $\hat{\rho} = \rho$. There is a mandatory condition; the term $\Sigma^T \Gamma + \Gamma \Sigma$ has to be definite negative due the other term that is part of the equation (46) is $(KH)^T \Gamma$.

The equation (45), that represents the reaction kinetic estimator, has an equivalent structure to the Luenberger observer used on homogeneous reaction systems [1].

$$\dot{\hat{\xi}} = \underbrace{A\hat{\xi} + Bu}_{1^*} + \Omega(\xi - \hat{\xi}). \tag{47}$$

The highlighted section 1* on the previous equation, is equivalent to the one shown on the equation (45).

$$\dot{\hat{\xi}} = \underbrace{KH\hat{\rho} - D\xi - Q + F}_{1^*} - \Omega(\xi - \hat{\xi}). \tag{48}$$

The previous equation (48) represents the non-linear system, however the equation (47) is the equivalence of the linearized system.

Some conditions must be fulfilled to perform the implementation. First, the matrix Γ should be squared and could be dependent on ξ; however, it must be stable for all ξ. Second, the current values on ξ are the same used on the equation (45). The data comes from direct measurements over the anaerobic reactor and data estimation. Finally, the current value of ρ, unknown at the time, is being replaced by the same equivalent estimated $\hat{\rho}$. The equation (46) shown the formula. Ω is the gain matrix used to influence the convergence of $\hat{\rho}$.

Matrices Ω and Γ are design parameters that affect the stability properties. A typical value selection is to take.

$$\Omega = diag\{-w_i\}, \quad para \ i = 1, ..., N \tag{49}$$

with.

$$\Gamma = diag\{\gamma_j\}, \quad para \ j = 1, ..., r \tag{50}$$

3.3.1. Observer Design

Only one reference must be followed to design the kinetic reaction estimator; the measured and estimated states on $\dot{\zeta}$. The term $\zeta - \hat{\zeta}$ is used as a reference to monitor and follow the estimator's performance. The aim is that the value of $\hat{\zeta}$ converges to ζ as soon as possible ($\zeta \approx \hat{\zeta}$). The dynamic of $\hat{\zeta}$ depends on the evolution of the dynamic of the error $\dot{e} = (A - \Omega L)e$. Thus, the references (the known values) that assist in tuning the kinetic reaction estimator are ζ, $\hat{\zeta}$, K, and H. Following some definitions are proposed.

- $e = \zeta - \hat{\zeta} \rightarrow$ Observation error
- $\tilde{\rho} = \rho - \hat{\rho} \rightarrow$ Tracking error

Hence, using the following equations.

$$\dot{\hat{\zeta}} = KH\hat{\rho} - D\zeta - Q + F - \Omega(\zeta - \hat{\zeta}) \tag{51}$$

$$\dot{\zeta} = K\phi - D\zeta - Q + F \tag{52}$$

And deriving in both sides of the observation error and the tracking error, it results in $\dot{e} = \dot{\zeta} - \dot{\hat{\zeta}}$ and $\dot{\tilde{\rho}} = \dot{\rho} - \dot{\hat{\rho}}$. Taking the equations (51) and (57) and replacing them on the dynamic of $\dot{e}$.

$$\dot{e} = K\phi - D\zeta - Q + F - KH\hat{\rho} + D\zeta + Q - F + \Omega(\zeta - \hat{\zeta}) \tag{53}$$

$$\dot{e} = K\phi - KH\hat{\rho} + \Omega e \tag{54}$$

$$\dot{e} = KH\rho - KH\hat{\rho} + \Omega e \tag{55}$$

$$\dot{e} = KH(\rho - \hat{\rho}) + \Omega e \tag{56}$$

$$\dot{e} = KH\tilde{\rho} + \Omega e \tag{57}$$

In the same way the dynamic of the tracking error is as follows.

$$\dot{\tilde{\rho}} = -(KH)^T \Gamma e + \frac{d\rho}{dt}. \tag{58}$$

Putting the equations (57) and (58) on the same structure results in the following dynamic system.

$$\begin{bmatrix} \dot{e} \\ \dot{\tilde{\rho}} \end{bmatrix} = \begin{bmatrix} KH\tilde{\rho} + \Omega e \\ -(KH)^T \Gamma e + \frac{d\rho}{dt} \end{bmatrix} \tag{59}$$

After organizing the previous dynamic system results on the following equation system.

$$\begin{bmatrix} \dot{e} \\ \dot{\tilde{\rho}} \end{bmatrix} = \begin{bmatrix} \Omega & KH \\ -H^T K^T \Gamma & 0 \end{bmatrix} \begin{bmatrix} e \\ \tilde{\rho} \end{bmatrix} + \begin{bmatrix} 0 \\ \frac{d\rho}{dt} \end{bmatrix}, \tag{60}$$

using the following matrices.

$$A = \begin{bmatrix} \Omega & KH \\ -H^T K^T \Gamma & 0 \end{bmatrix} \tag{61}$$

$$V = \begin{bmatrix} 0 \\ \frac{d\rho}{dt} \end{bmatrix} \tag{62}$$

results in.

$$\begin{bmatrix} \dot{e} \\ \dot{\tilde{\rho}} \end{bmatrix} = A \begin{bmatrix} e \\ \tilde{\rho} \end{bmatrix} + V \tag{63}$$

According to the information described above, the equations 51 and 57 are divided into the correspondent submatrices to start classifying the estimation procedure as follows.

$$K_a = \begin{bmatrix} -k_1 & 0 \\ k_2 & -k_3 \end{bmatrix}, \quad K_b = \begin{bmatrix} 1 & 0 \\ 0 & 1 \end{bmatrix}, \quad F_a = \begin{bmatrix} DS_{1in} \\ DS_{2in} \end{bmatrix}, \quad F_b = \begin{bmatrix} 0 \\ 0 \end{bmatrix}. \tag{64}$$

The next step is to calculate the matrix A_0 that comes from the equation (25), then.

$$A_0 = -K_b K_a^{-1}. \tag{65}$$

Following, the system is divided into the dynamic states that want to be estimated and using the data estimated by the asymptotic observer, Z_1 and Z_2, and the measured data S_1 and S_2. Solving ξ_b from the equation (22), then.

$$\xi_b = Z - A_0 \xi_a. \tag{66}$$

The previous equation able to calculate the following matrices.

$$K = \begin{bmatrix} K_b \\ K_a \end{bmatrix}, \quad H = \begin{bmatrix} 1 & 0 \\ 0 & 1 \end{bmatrix}, \quad \xi = \begin{bmatrix} \xi_b \\ S_1 \\ S_2 \end{bmatrix}, \quad F = \begin{bmatrix} F_b \\ F_a \end{bmatrix} \tag{67}$$

Finally, all information needed to supply the equations (45) and (46) are obtained above.

4. Nonlinear Model Predictive Controller (MPC)

As it is shown on Figure 4 the observer structure calculates the non-measurable dynamic states, X_1 and X_2 (with the asymptotic observer), and the kinetic reaction rates r_1 and r_2 (with the reaction rates observer). Once the information of both measurements and virtual sensors has been delivered to the MPC controller, the operational and physical instructions, as well as the control objectives, are delivered too.

4.1. Controller design

According to the industrial requirements, essential to trace the deployment of the technology around the anaerobic digestion in the industry; the subsequent conditions are required to take into consideration.

- The reactor has to be balanced against perturbations, always working within physical and operational constraints.
- Methane production needs to be maximized all the time.
- Environmental regulations should be followed according to local regulations criteria; $S_1(t) + S_2(t) \leq Kt_d$. Kt_d denotes the maximum effluent concentration of both substrates considered.
- The reactor has to be protected against failures due to unexpected variations on VFA and, therefore, periodically drops on pH. Once it happens, there is no available route to bring the reactor back towards a regular operation. The following equation emerges as a condition to contain, during operation, the amount of VFA with a sufficient amount of Z. It is called the buffer capacity; the ability to regulate the values of S_2 and Z to maintain the system under operation.

$$\frac{S_2(t)}{Z(t)} = \lambda \tag{68}$$

Researchers suggest that the range values of λ usually have to be within 0.1 and 0.3 [13].

4.2. Structure of the controller

The control structure proposed is shown in Figure 5. The dilution rate D is the manipulated variable, and the outputs selected are the biogas flow rate (q_m), the organic substrate

concentration (S_1), the VFA concentration (S_2), and the total alkalinity (Z). All information from reactor; measurements, n_{med}, pH, and the estimated dynamic states, X_1, and X_2, as well as the kinetic reaction rates, r_1 and r_2. The optimization algorithm, using all inputs and based on the mathematical model, calculate the optimal dilution rate D based on a prediction of the future over a horizon.

Using the mathematical model that describes the anaerobic digestion (AD) process, this paper proposes the following optimal controller algorithm.
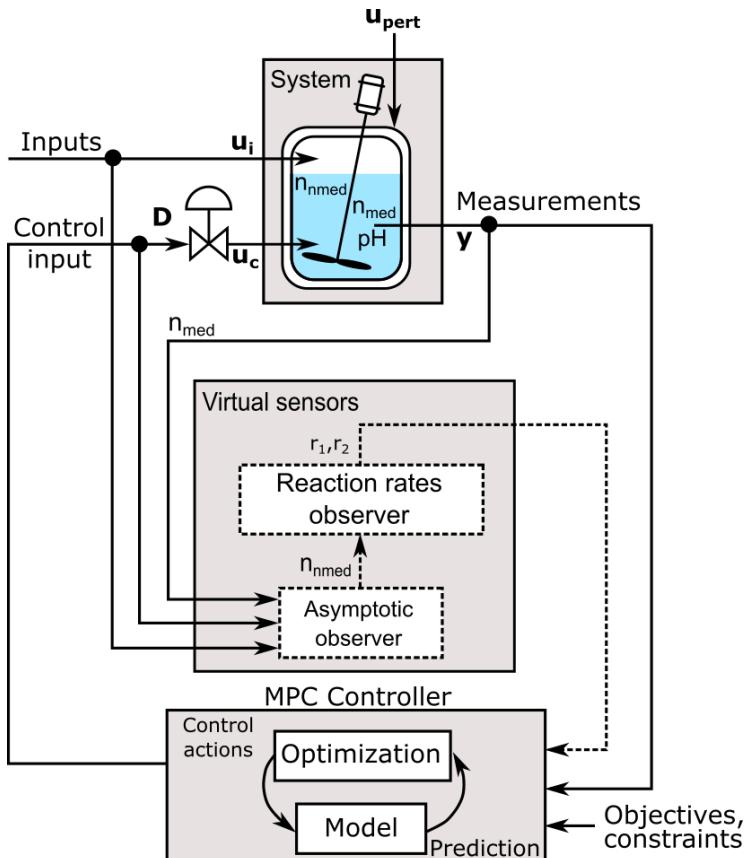
Figure 5. MPC controller with the observer structure.

$$\max_{u(k),...,u(k+N_c)} J(u(k), y(k), w(k)) \tag{69}$$

sujeto a:

$$
\begin{aligned}
&x(k+1) = f(x(k), u(k)), \\
&y(k) = g(x(k), u(k)), \\
&x_{min} \leqslant x(k), \forall k = 1, ..., N_p \\
&u_{min} \leqslant u(k) \leqslant u_{max}, \forall k = 1, ..., N_u \\
&\frac{S_2(k)}{Z(k)} \leqslant \lambda, \forall k = 1, ..., N_p
\end{aligned}
\tag{70}
$$

where $J(\cdot)$, $x(k)$, $y(k)$, $w(k)$, $g(\cdot)$ and $f(\cdot)$ are the functional cost that contains the control objectives, the dynamics of the system, the outputs, the reference signal the function of the output and the mathematical model of the system respectively [16]. The following is the functional cost proposed.

$$J(u(k), y(k), w(k)) = \sum_{i=1}^{209} X_2(i)\mu_2(i)k_6 \tag{71}$$

The equation above is the sum, along the simulation, of the total volume of methane produced by the anaerobic digestion. x_{min} are the lower boundaries of the dynamics states. u_{min} and u_{max} are the control action variable's lower and upper boundary limits, the dilution rate D, between 0 and 1. The last condition, the buffering capacity, will be programmed with different values to test the performance of the system.

Two variations of the proposed MPC controller are considered for testing the main characteristics. The emphasis relates to the maximization of the volume of methane produced to evaluate controllers' performance. The first MPC controller is programmed to run without any operational restrictions. Used as a reference, this alternative aims to explore improvements and drawbacks, checking the progress of leading indicators under stressful operational situations. The second MPC controller uses all operational restrictions shown on (70). Both configurations are tested with and without multi-start. In order to evaluate the improvement achieved by the MPC controller proposed, the volume of methane produced and other phenomenological effects will be tested with traditional PID industrial controllers [17].

5. Simulation results and analysis

First of all, this chapter evaluates the estimation of both; the non-measurable state dynamic variables and the kinetic reaction rate parameters. The results achieved established a link of confidence between the variables measured and the information required by the mathematical model. Second, once the flow of information is considered reliable, the MPC controller proposed is ready to be tested by traditional implementations in the industry [16].

5.1. Simulation conditions

This section employs the same profile inputs and initial conditions used in the parametric identification procedure. In the following Table 3 the initial conditions of the state dynamics are shown.

Table 3. Initial conditions of state variables.

	$X_1(0)$	$X_2(0)$	$S_1(0)$	$S_2(0)$	$Z(0)$	$C(0)$
Valor	0.55	0.5	17	3.4	10.7	8
Unidades	[g/L]	[g/L]	[g/L]	[mmol/L]	[mmol/L]	[mmol/L]

Figure 6 shows the profile inputs used along the 209 days of simulation.

5.2. Asymptotic observer

There is one significant problem due to the use of control and monitoring systems; it is not yet possible to achieve all measurements online to feed the mathematical model and run a controller. In order to confront this, the first step is to start the operation of an asymptotic observer to estimate the dynamic state variables concentration of acidogenic X_1 and methanogenic X_2 bacterias. This category of observers is named asymptotically because it estimates the non-existing measurable states based on two conditions; the system is still not exponentially observable, and the reaction kinetics are unknown.

Figure 7 shown the results obtained by the algorithm. To test the performance of the observer, the values of the estimations were compared with the dynamic measured directly from the mathematical model. The starting point of the observer and the mathematical model were different in order to confirm the dynamics will converge sometime.

5.3. Kinetic parameter reaction estimator

The good performance of the estimated state variables X_1 and X_2, achieved by the asymptotic observer, far exceeds the minimum standard requirements to make its use possible. Then, is it possible to unlock the algorithm that estimates the kinetic parameters, r_1 and r_2, because they depend on the information coming from all dynamic state variables. These variables are used as a reference to determine the convergence of the estimator, see Figure 7. A practical test of the estimator makes the initial conditions of the kinetic parameter estimator and the mathematical model different. The convergence of both determines the degree of accuracy. At the same changes on dilution rate D, at days 50 and 100, both the measured dynamics and the estimates, X_1 and X_2 follow in the same course and tendency [18,19].
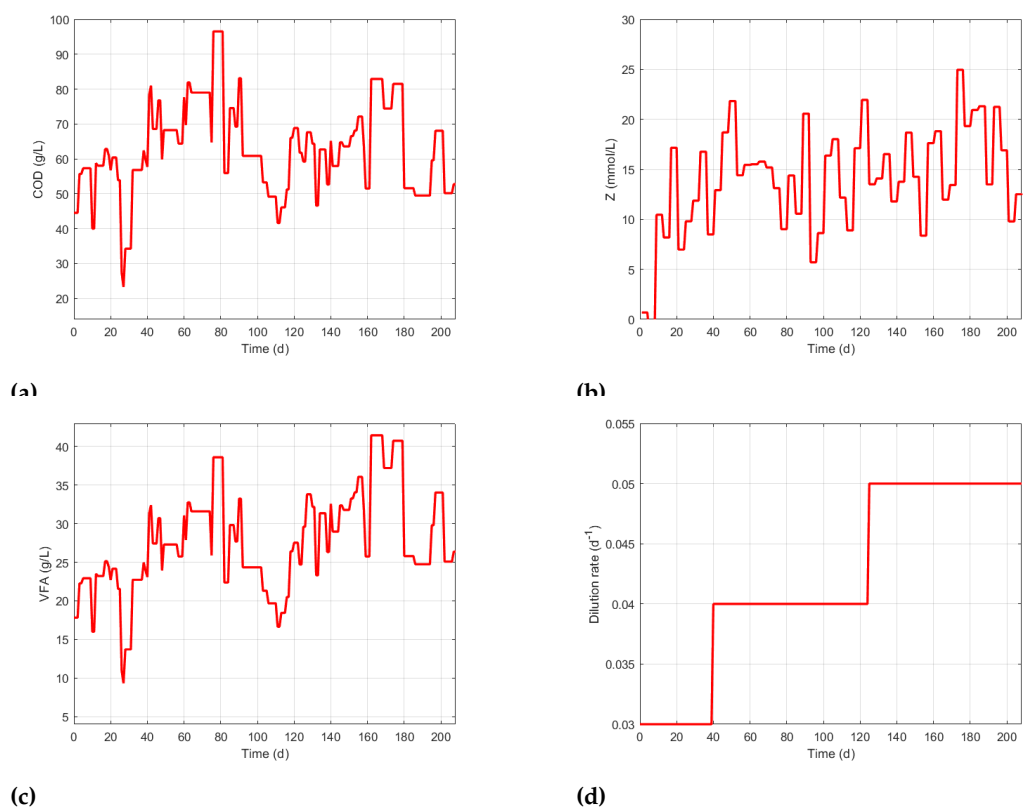
Figure 6. Data profile inputs used on influent. (**a**) volatile fatty acids (VFA); (**b**) chemical oxygen demand (COD); (**c**) level of pH; (**d**) alkalinity (Z).
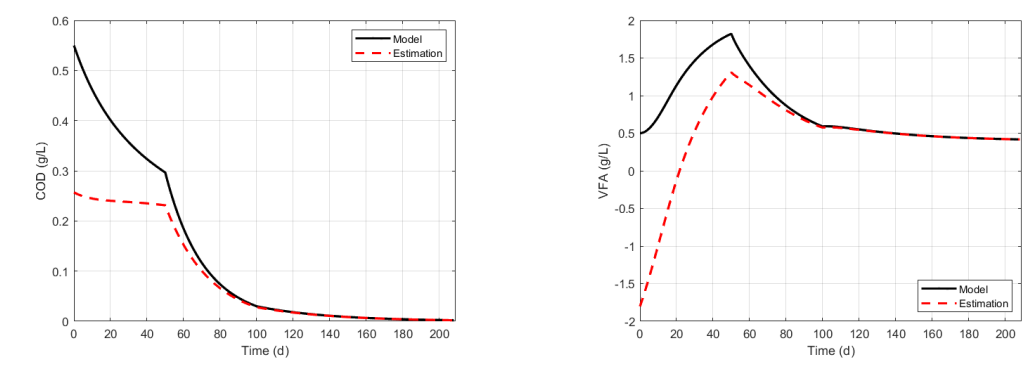
Figure 7. Asymptotic observer for state dynamic variables X_1 and X_2 estimated compared with measured values.

Both, the observed and measured kinetic reaction parameters, r_1 and r_2, are shown on Figure 8. Due to a scale factor, it is not possible to take a closer look at the difference in initial conditions. However, the figure allows a straightforward comparison of the magnitudes of the kinetic reaction rate parameter from the mathematical model and the correspondent estimation. Similarly, on days 50 and 100, the change in dynamics is appreciated. The value of the dilution rate D changed from 0.03 to 0.07. However, the important thing is to appreciate the convergence between the values. Figure 9 take a deeper look at the results. As expected, after a few days, the magnitudes become very similar.

(a)   **(b)**
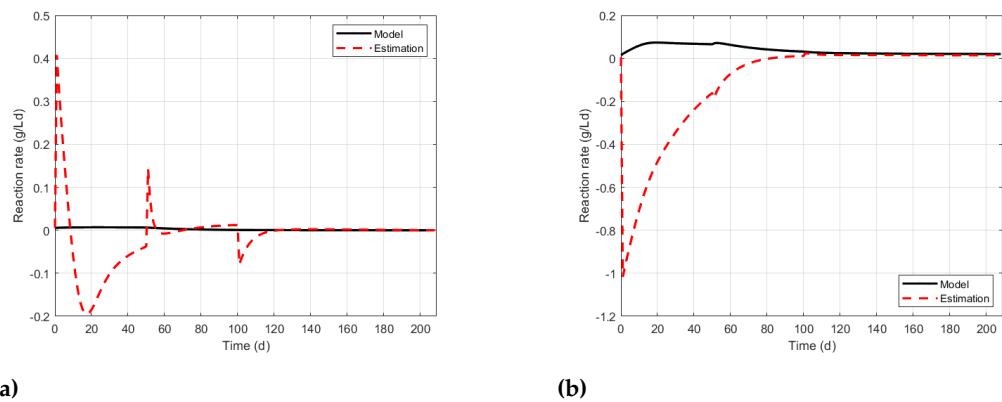
Figure 8. Asymptotic observer for reaction kinetic r_1 and r_2. (**b**) Influent alkalinity results using the algorithm step-ahead.

The results of all dynamic state variables considered by the observer are shown in Figure 10. As expected, due to the dynamic states S_1 and S_2 being measured, these magnitudes are the same compared to the estimated ones. However, dynamic states and the estimated values (X_1 and X_2) effectively converge a few days later. Finally, Figure **??** shows the relative errors associated with the previous results.

(a)   **(b)**
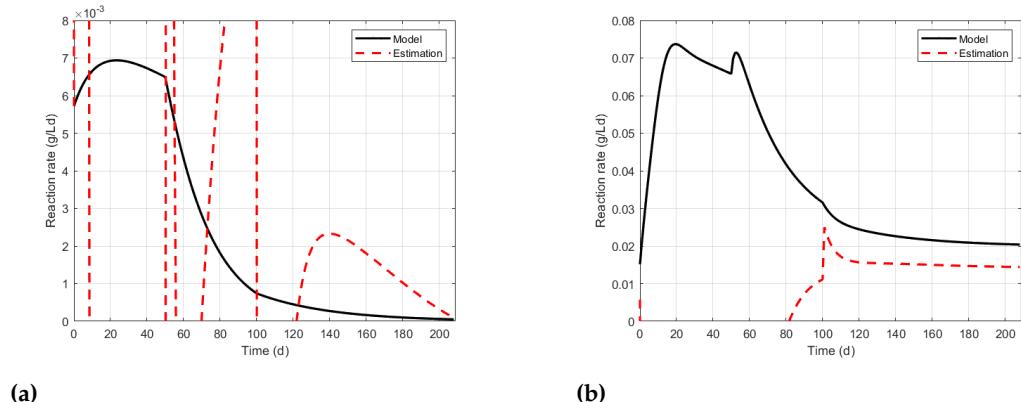
Figure 9. Scale augmentation on Figure 8 in order to validate details over the convergence process.

5.4. PID Controller Performance on Aanerobic Digesters

This section explores the performance of PID controllers used in the anaerobic digestion industry in order to establish a baseline that assists the objective of quantifying the improvements achieved by the MPC controllers proposed in this paper.

The PID control scheme proposed is tested in a wide range of operational scenarios to evaluate its robustness against different circumstances. The control actions calculated will depend on the following changes on the reference; moderate, medium, and extreme variations on the total volume of CH_4 produced, see Figure . The changes were conducted on the day 50 and remained constant for 50 days until day 100. Next, the reference goes

back to the previous value to check the system's capacity to recover the previous stability   443
conditions (see black line). The discontinuous blue line represents the volume of methane   444
produced by the reactor using the profile inputs from Figure 6. The objective is to use the   445
result as a reference in the background to contrast the performance of the PID controller   446
(discontinuous red line). Figures 12a and 12b show the capacity of controller to follow the   447
reference with small oscillations. In two stages, the controller stays around on a stable   448
region (when the values change to 18 m^3/d and 28 m^3/d respectively). Nevertheless, Figure   449
12c show that the controller is not capable to follow up the desired reference (when the   450
values change to 43 m^3/d). The system falls into a destabilization region, where methane   451
production dropped below even when the reference returned to the previous state. Thus,   452
the information on the physical and operational conditions of the anaerobic digester are   453
not inserted into the controller algorithm; the allowed bio-chemical restrictions are not   454
considered; consequently, the system works outside the permissible range.   455

(a)

(c)   (d)
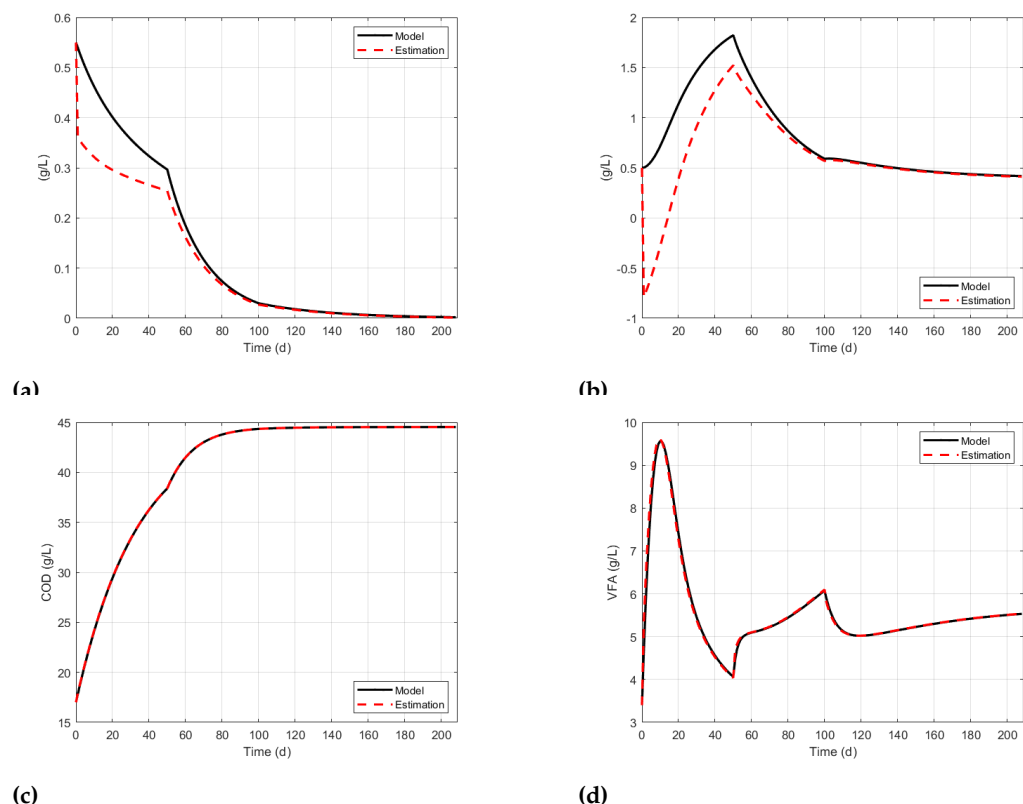
Figure 10. Kinetic reaction estimator to state variables considered. (**a**) volatile fatty acids (VFA); (**b**) chemical oxigen demand (COD); (**c**) level of pH; (**d**) alkalinity (Z).

The correspondent value of dilution rate D is shown on Figure 13. Figures **??** and **??** show   456
normal operation until day 100, when the system crashed, because the value of D dropped   457
below zero and go beyond operational regions over limits. Figure 14 shown the value of pH 458
for the correspondent cases. Once again, the values of pH linked using the PID controller   459
operate beyond the right limits. The previous analysis induces to prepare future actions to   460
oppose resistance drawbacks related to unusual values of S_2.   461
  462

Figure 15 shows the value of λ along the simulation for the three correspondent cases.   463
Below the limit recommended (0.8) by some authors on literature, fortunately, λ in the   464
first two cases (Figures and) correspond to a correct values. However, when the limits are   465
exceeded, Figure shows that the value of S_2 far exceeds the limits, having values of λ close   466
to 4. As was stated in previous results, the PID controller cannot manage the system within   467
physical and operational boundaries. Based on previous results, the alternative proposed   468

in this paper, the MPC controller, becomes a reasonable alternative because its algorithm considers some valuable characteristics of the homogeneous reactions system [20].

5.5. Controlador MPC sin restricciones

5.5.1. Sin función multistart

Figures 16 and 17 shown the results obtained due the operation of MPC controller without the restriction buffering capacity (λ).

(a)

(b)

(c)

(d)
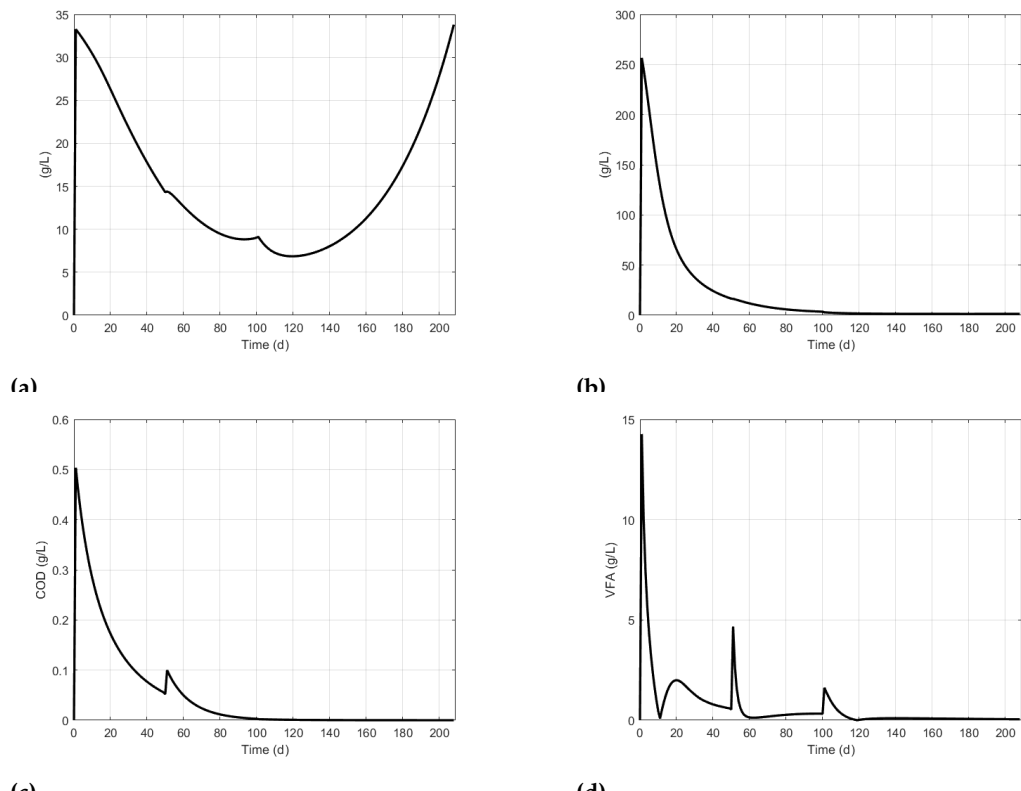
Figure 11. Error during the estimation process of reaction kinetics for. (**a**) volatile fatty acids (VFA); (**b**) chemical oxigen demand (COD); (**c**) level of pH; (**d**) alkalinity (Z).

Figure 16a shows the volume of methane produced by both the reference (black line), the system with the input profiles from Figure 6 and the MPC controller without operational restrictions (discontinuous red line). Figure 16a shows a significant increase in the volume of methane produced almost always along the reference. Figure 16b shows the profile assumed as a reference (black line). The discontinuous red line shows the control actions calculated by the MPC controller. The oscillation is severe along the simulation; however, the results are reliable and work well. Figures 16c and 16d shown the results of the level of pH and S_2. As is expected, the oscillation of values (discontinuous red line) are intense around the reference (black line) but not attractive for control purposes. Finally, Figure 17a shown the evolution of the non restricted parameter λ. As expected, the maximum value of λ (discontinuous blue line) was exceeded once. According to previous description, Figure shown the relation between the state variables S_2 and Z [1,13].

5.5.2. With multistart function

On the other hand, Figures 18 and 19 show the results of adding the multi-start function, which is supposed to be an improvement of the previous algorithm. Figure 18a shown an increase in the volume of methane produced in comparison with Figure 16a.

The system had to increase the strength of movements around the input controlled variable D (see Figure 18b), and the oscillation is severe between limits 0 and 0.1. In the same way,

(a)

(b)

(c)
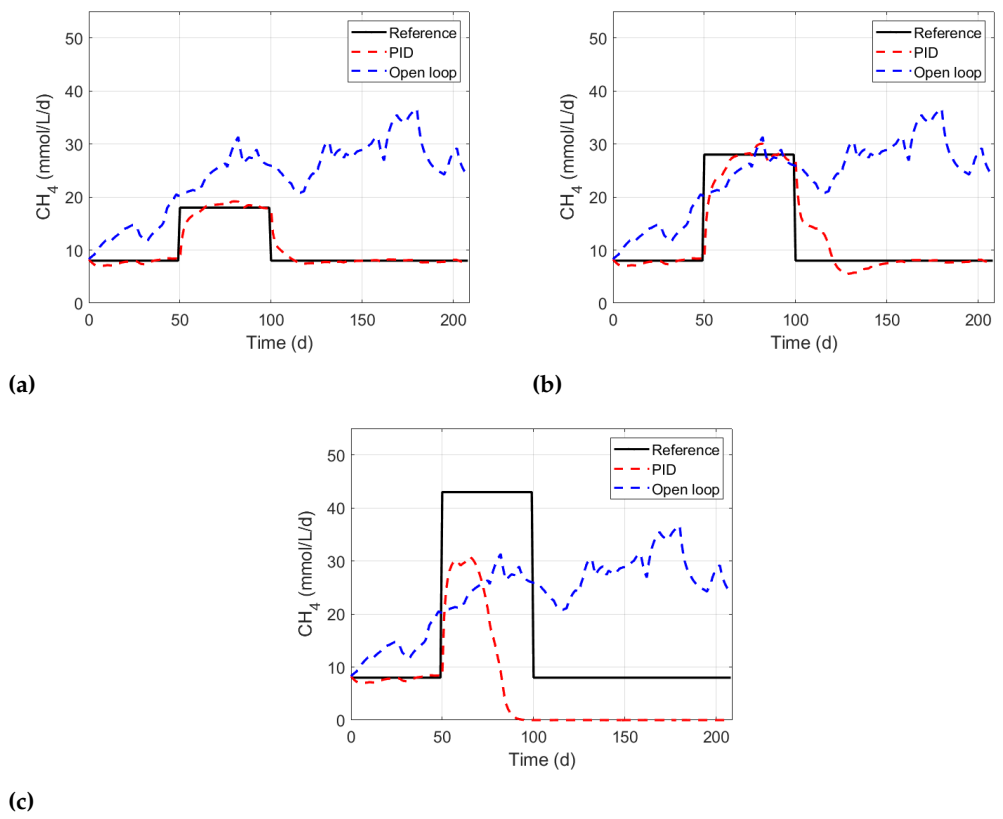
Figure 12. Three different references to follow of methane produced using a PID controller.

(a)

(b)

(c)
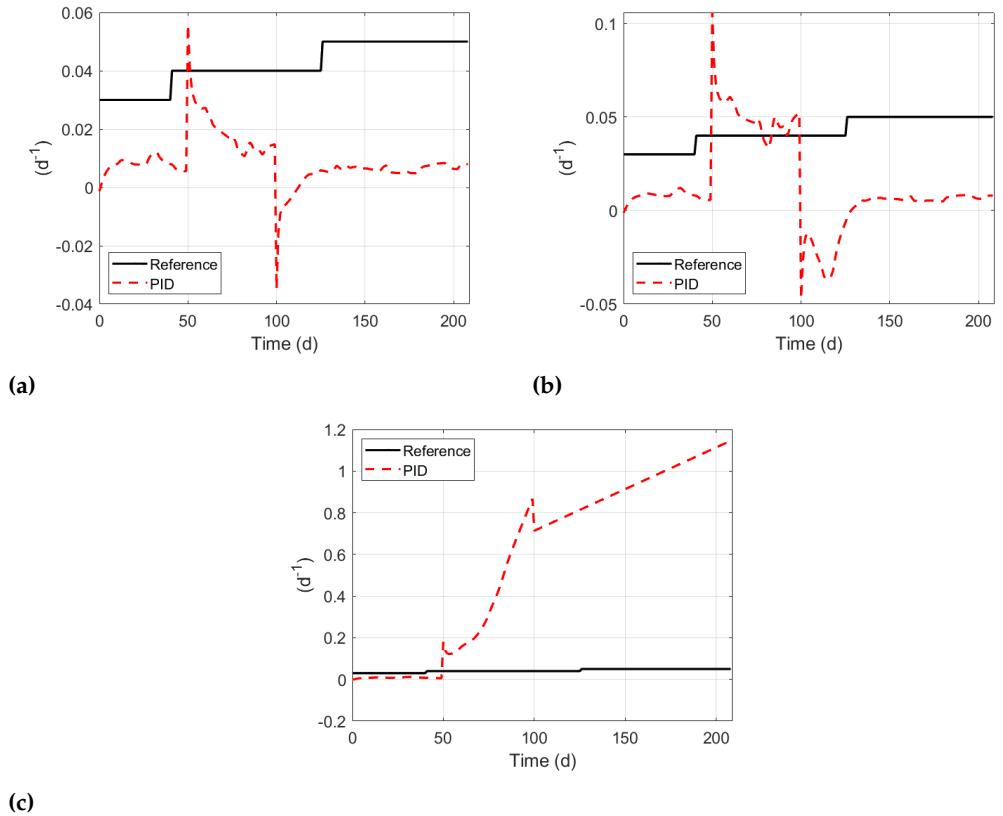
Figure 13. Dilution rate D results related to the volume of methane (CH_4) produced by PID controller.
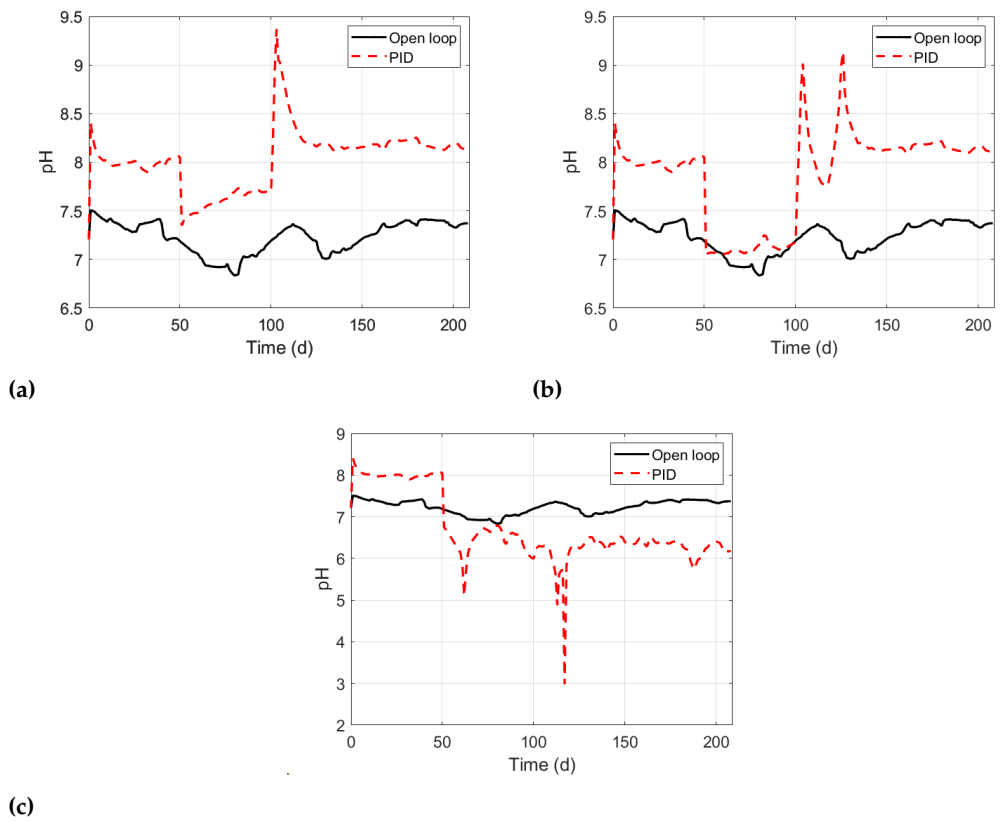
Figure 14. Evaluation of the pH level over the three different scenarios using a PID controller.
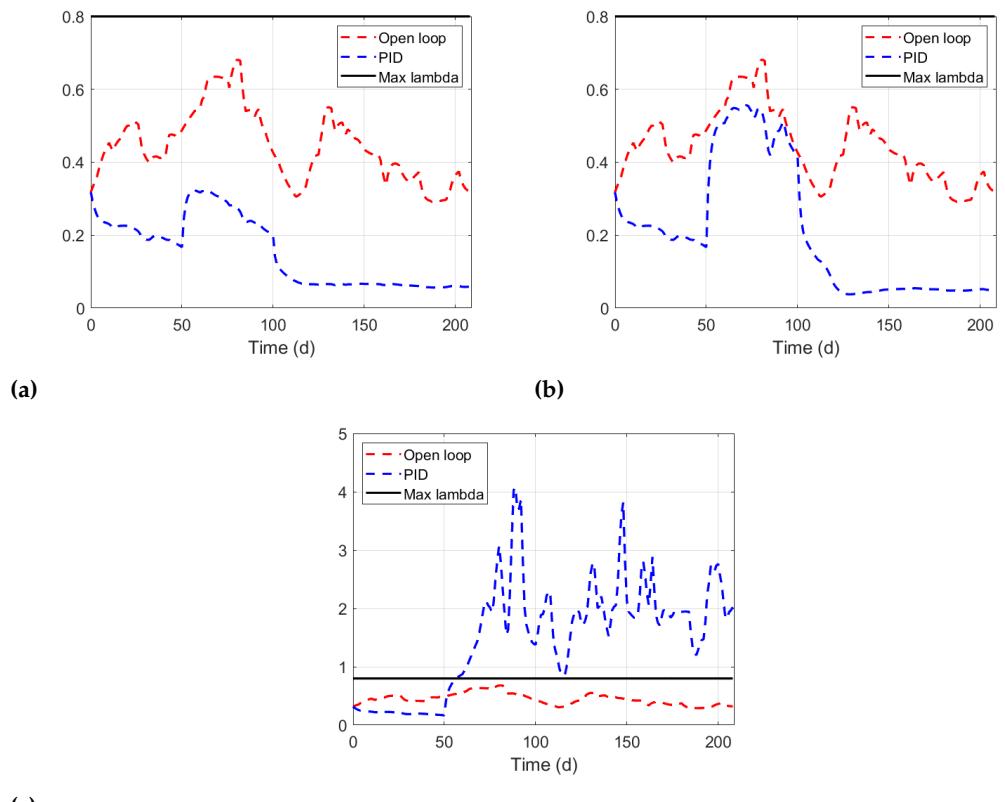
Figure 15. Value of λ over the three different scenarios considered.

the level of pH had severe changes even beyond feasible operational regions (see Figure 18c); hence it causes similar variations in the value of the amount of acid produced S_2, see Figure 18d. Figure 19a, shown the value of λ along the simulation. It goes beyond the limit repeatedly. Figure **??** shows even the value of alkalinity Z even when it exceeded the value of S_2, meaning that the value of λ goes beyond 1. Given the previous results, the maximization of the volume of methane produced leads the system towards no feasible operational regions, it is necessary to include operative restrictions to avoid inhibitions produced by the presence of acids.

(a) **(b)** **(c)** **(d)**
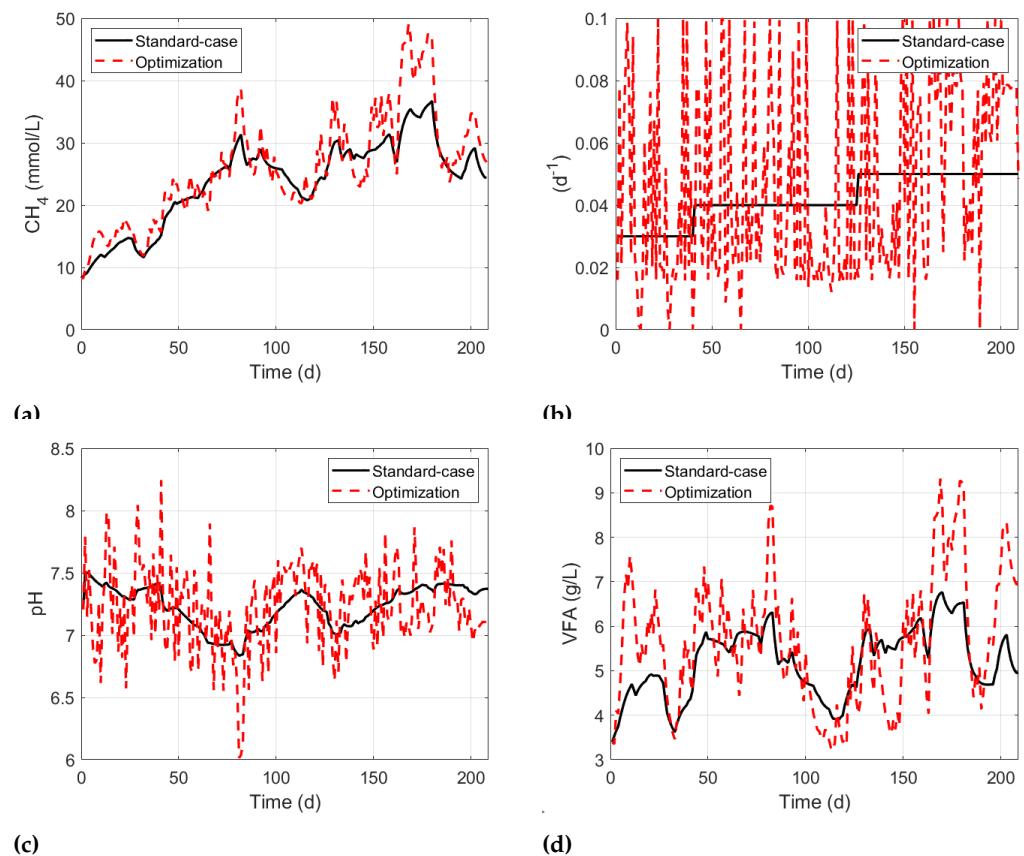
Figure 16. Results of the MPC controller without restrictions maximizing the amount of CH_4 produced.

(a) **(b)**
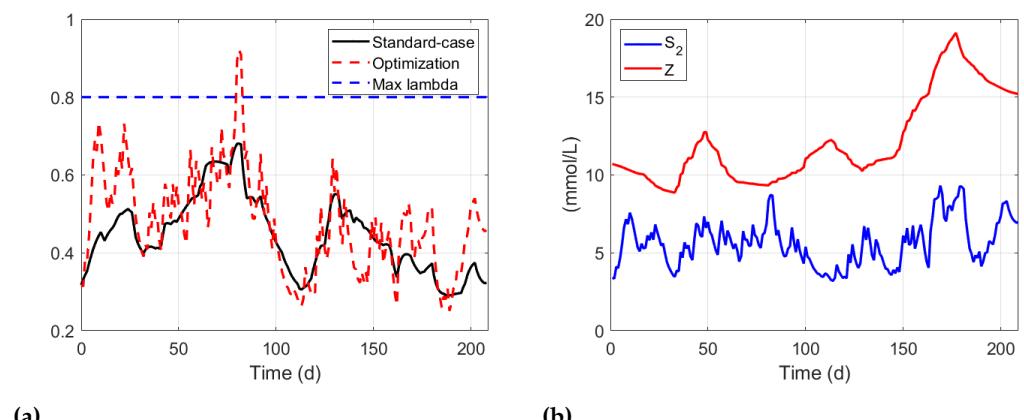
Figure 17. Results of the MPC controller without restrictions maximizing the amount of CH_4 produced.

5.6. MPC controller with restrictions

5.6.1. Without multistart function

In the following figures the algorithm of the MPC controller includes the operation restriction of buffering capacity λ.

(a)   **(b)**

(c)   **(d)**
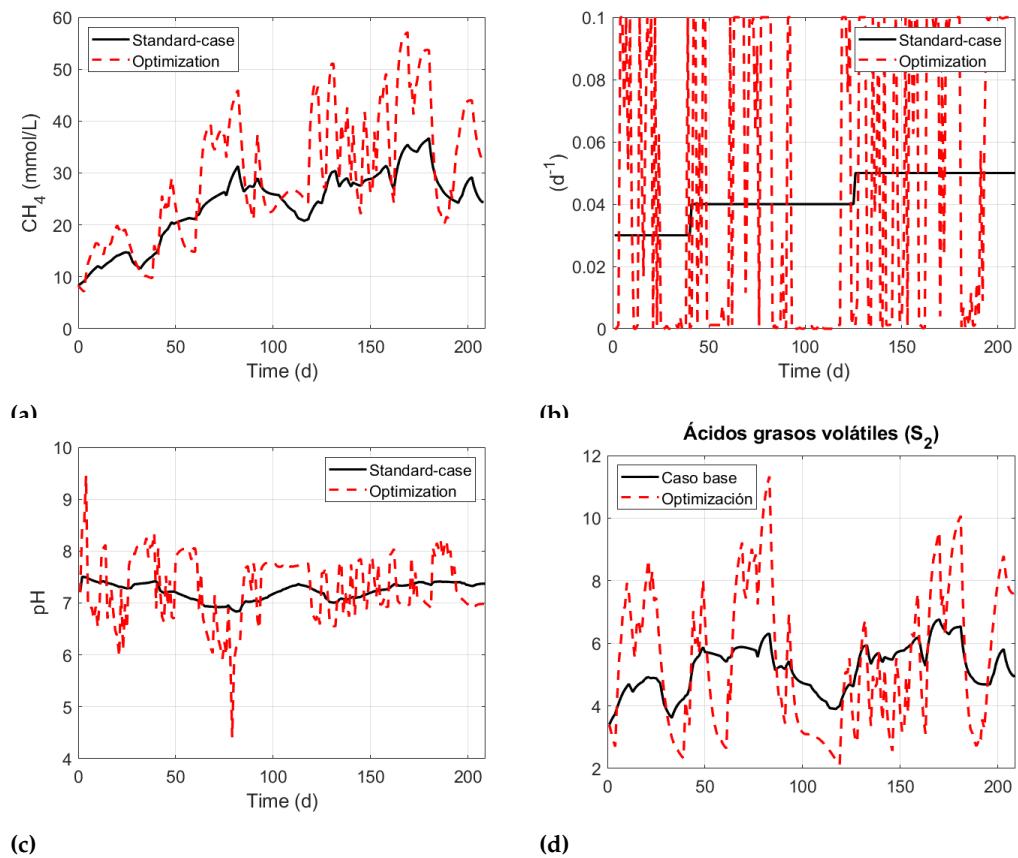
Figure 18. Results of the MPC controller without restrictions with multistart maximizing the amount of volume of C_{H4}.

(a)   **(b)**
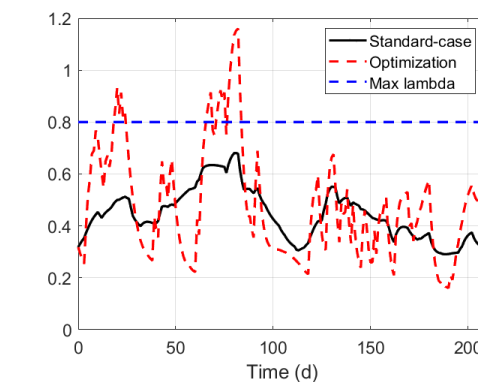
Figure 19. Results of the MPC controller without restrictions with multistart function maximizing the amount CH_4 produc ed.

Now, the value of the operational limit λ is restricted to 0.8. Figures 20 and 21 shown the results. Although the algorithm is restricted, the amount of methane CH_4 produced is higher than the reference. Figure 20a shown the control actions calculated. However, as seen on Figures 20c and 20d the oscillations are extreme on the level of pH and S_2 compared with previous results.

Figure 21a shows how operational restrictions work adequately over the feasible region, where the value of λ works below 0.8. Figure 21b evidence the aforementioned behavior. The previous condition helped the system to have enough space to allow the control algorithm to increase the value of dilution rate D if required. In the following section, the objective is to improve the results by increasing the probability of finding the best values for the methane produced with the multi start function.
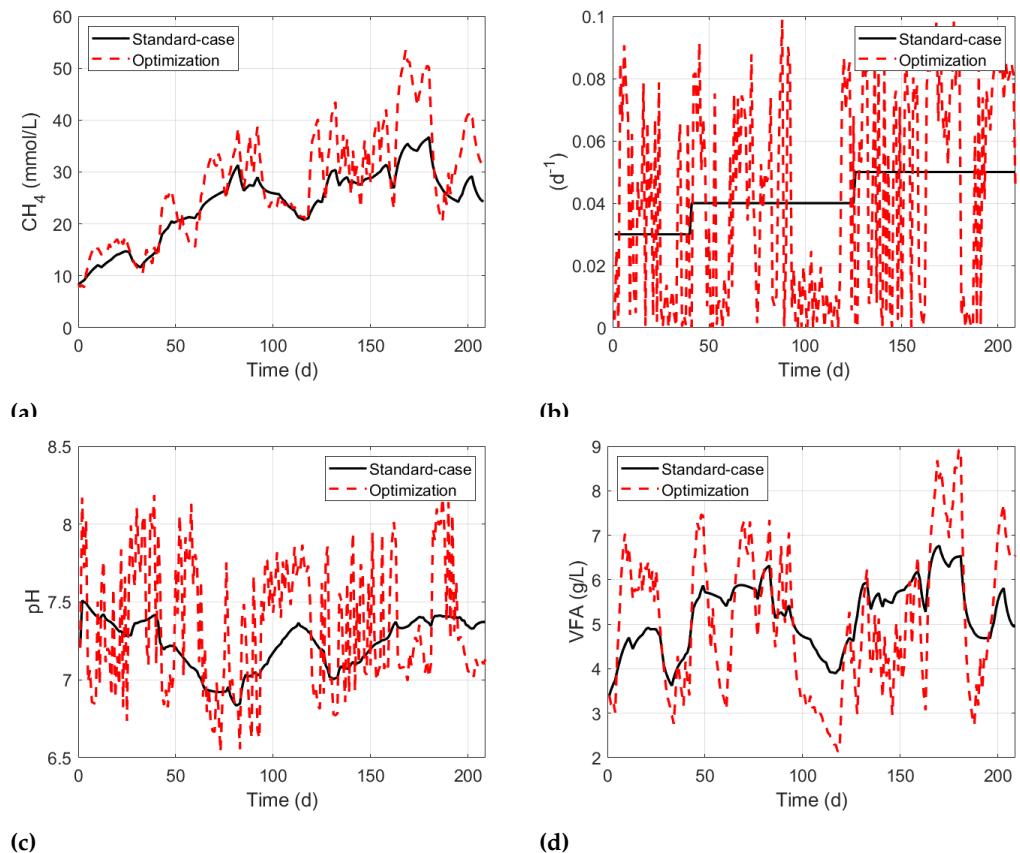
Figure 20. Results of the MPC controller with restrictions maximizing the volume of the CH_4 produced.
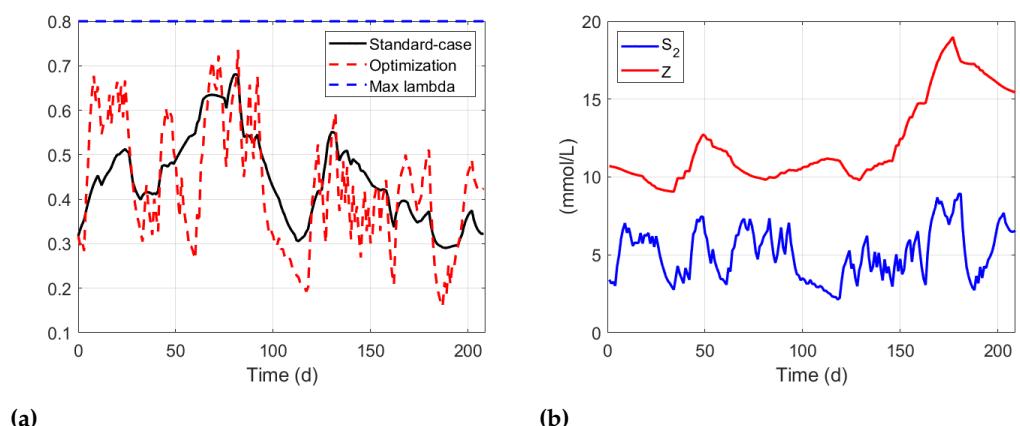
Figure 21. Results of the MPC controller with restrictions maximizing the flow of methane CH_4 produced.

5.6.2. With multistart function

Figures 22 and 23 shown the potential to produce methane under restricted scenarios with multi-start function. As shown in Figure 22a, the discontinuous red line is higher than the results shown in the previous section.
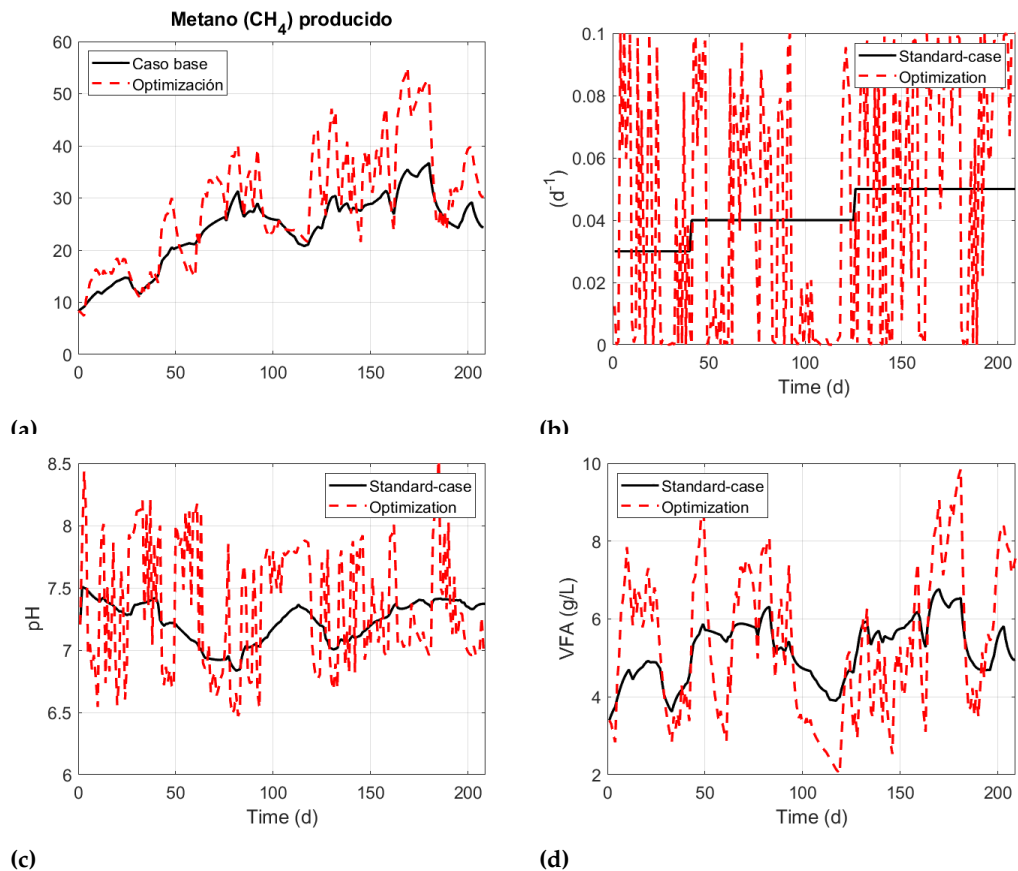
Figure 22. Results of the MPC controller with restrictions using the multistart function maximizing the volume of CH_4 produced.

The rest of Figures 22b, 22c and 22d shown a similar behaviour as the previous results, however, with only a slight difference but an increase in performance. Figure 23a shows that control actions calculated by MPC have been taken to extremes but maintaining the parameter λ under the limits.

Table 4. Improvement on performance over production of CH_4 for the MPC control schemes.

	Sin restricciones		Con restricciones	
	Sin multistart	Con multistart	Sin multistart	Con multistart
% Mejora	17.40	24.41	18.82	20.85

Finally, Table 4 shows a condensed vision of the previous results. The results, used as a reference, are the volume of methane CH_4 produced, shown by the black line along the four MPC performance tests. In the case of the MPC controller that works without operational restrictions, the improvement achieved was 17.40% and 24.41% both, with and without using the multi-start function, respectively. However, the reactor must operate under feasible operational restrictions (where inhibitions and drawbacks caused by acids are avoidable), no matter whether the performance is compromised. The improvement achieved by the MPC controller that works with operational restrictions was 18.82% and 20.85% both with and without using the multi-start function. Although performance is reduced significantly because of the insertion of restrictions in the algorithm (due to the

revenue produced by the amount of methane CH_4 produced decreases), the operation of the reactor does not be unbroken anymore, and it runs constantly.

(a)   **(b)**
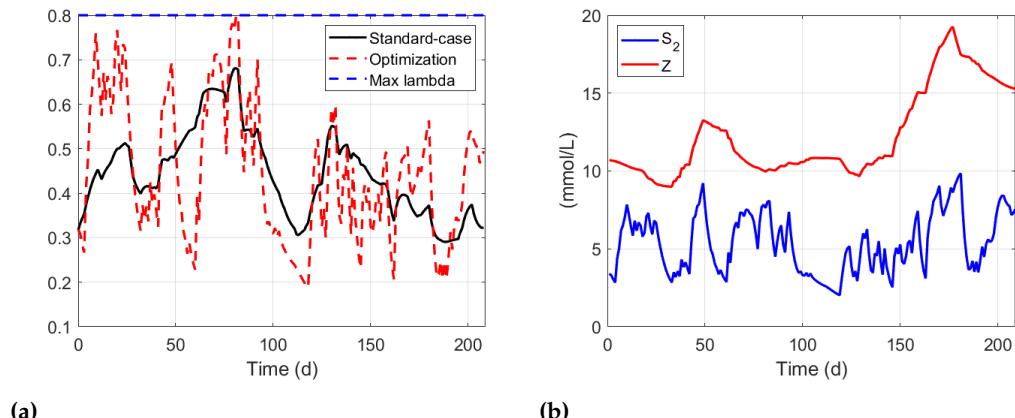
Figure 23. Results of the MPC controller with restrictions and multi-start function maximizing the volume of CH_4 produced.

6. Conclusions

The main results of this paper were to make it possible to put together the three leading solutions that come together and result in a successful operation of a monitor and control system structure in concise and fluidized operation. The first element is the core of the algorithm; the way and connections used to construct (or represent) the phenomenon, the mathematical model with parameters identified over experimental data using optimization-based algorithms. The second element is the observer structure of state dynamics and kinetic reaction parameters that reconstruct non-measured data due to drawbacks from the absence of reliable sensors. Finally, the third element is an MPC controller with restrictions over the reaction system that guarantees straight operation far from unfeasible scenarios of inhibition due to the presence of acids. In addition to the above, it was possible that a high increment in the volume of methane CH_4 produced using this scheme.

With close monitoring of the main contributions aforementioned, the parameter identification algorithm's success resulted from using the step-ahead strategy. Using genetic algorithms was the first step in adjusting the mathematical model so close to the data from the experiment. Finally, the structure composed by an asymptotic observer demonstrates a valuable tool to recover the lack of data from the concentration of acidogenic and methanogenic populations of bacterias. It was established to lay the first stone of the structure capable of estimating the kinetic reaction parameters, be of prime importance to following the variation of the kinetic reactions, previously considered as static; one of the main problems in the implementation of MPC control systems.

1.   Front Matter. In *On-line Estimation and Adaptive Control of Bioreactors*; Bastin, G.; Dochain, D., Eds.; Process Measurement and Control, Elsevier: Amsterdam, 1990.
2.   Song, Y.J.; Oh, K.S.; Lee, B.; Pak, D.W.; Cha, J.H.; Park, J.G. Characteristics of Biogas Production from Organic Wastes Mixed at Optimal Ratios in an Anaerobic Co-Digestion Reactor. *Energies* **2021**, *14*. doi:10.3390/en14206812.
3.   R., C.; H., T.; T., H. Hydrotermal pretreatment of rice straw biomass: A potential and promising method for enhanced methane production. *Appl. Energy* **2012**, *94*, 129 – 140.
4.   M., A.; N., B.; Srinivasan.; B..; D., B. Extents of reaction and flow for homogeneous reaction systems with inlet and outlet streams. *AIChE Journal* **2010**, *56*, 2873–2886.
5.   Monteiro, E.; Ferreira, S. Biomass Waste for Energy Production. *Energies* **2022**, *15*. doi:10.3390/en15165943.

6. Marquez-Ruiz, A.; Mendez-Blanco, C.; Porru, M.; Özkan, L. State and Parameter Estimation Based On Extent Transformations. *Computer Aided Chemical Engineering* **2018**, *44*, 583–588.

7. Marquez-Ruiz, A.; Mendez-Blanco, C.; Ozcan, L. Constrained Control and Estimation of Homogeneous Reaction Systems Using Extent-Based Linear Parameter Varying Models. *Industrial Engineering Chemistry Research* **2020**.

8. Condrachi, L.; Vilanova, R.; Meneses, M.; Barbu, M. Anaerobic Digestion Process Control Using a Data-Driven Internal Model Control Method. *Energies* **2021**, *14*. doi:10.3390/en14206746.

9. Andrews, J.F. A mathematical model for the continuous culture of microorganisms utilizing inhibitory substrates. *Biotechnology and Bioengineering* **1968**, *10*, 707–723.

10. Rossi, E.; Pecorini, I.; Ferrara, G.; Iannelli, R. Dry Anaerobic Digestion of the Organic Fraction of Municipal Solid Waste: Biogas Production Optimization by Reducing Ammonia Inhibition. *Energies* **2022**, *15*. doi:10.3390/en15155515.

11. Ahmad, F.; Jameel, A.; Kamarudin, M.; Mel, M. Study of growth kinetic and modeling of ethanol production by Saccharomyces cerevisae. *Afr J Biotechnol* **2011**, *10*.

12. Ardestani, F.; Kasebkar, R. Non-Structured Kinetic Model of Aspergillus niger Growth and Substrate Uptake in a Batch Submerged Culture. *British Biotechnology Journal* **2014**, *4*, 970–979. doi:10.9734/BBJ/2014/11472.

13. Hoil, K.; Li, D.; Yugeng, X.; Jiwei, L. Model predictive control with on-line model identification for anaerobic digestion processes. *Biochemical Engineering Journal* **2017**, *128*, 63–75.

14. Cortés, L.G.; Barbancho, J.; de la Rubia, M.A.; Larios, D.F.; Marín, J.D.; Mohedano, A.F. Extension of Usable Raw Sludges for Control Purposes on Anaerobic Digestion Reactors Using On-line Model Parameter Identification Strategy. *Sensors* **In process of submission**.

15. O., B.; Z., H.S.; D., D.; A., G.; J.P., S. Dynamical model development and parameter identification for an anaerobic wastewater treatment process. *Biotechnol Bioeng* **2001**, *75*, 424–438.

16. Valencia, F.; López, J.D.; Núñez, A.; Portilla, C.; Cortes, L.G.; Espinosa, J.; Schutter, B.D. Congestion Management in Motorways and Urban Networks Through a Bargaining-Game-Based Coordination Mechanism. *Springer* **2015**, pp. 1–40.

17. Batstone, D.; Keller, J.; Angelidaki, I.; Kalyuzhnyi, S.; Pavlostathis, S.; Rozzi, A.; Sanders, W.; Siegrist, H.; Vavilin, V. Anaerobic digestion model No 1 (ADM1). *Water science and technology : a journal of the International Association on Water Pollution Research* **2002**, *45*, 65–73.

18. Isaza-Hurtado, J.; Botero-Castro, H.; Alvarez, H. Robust estimation for LPV systems in the presence of non-uniform measurements. *Automatica* **2020**, *115*, 108901.

19. Batstone, D.; Keller, J.; Newell, B.; Newland, M. Model development and full scale validation for anaerobic treatment of protein and fat based wastewater. *Water Science and Technology* **1997**, *36*, 423–431. doi:10.2166/wst.1997.0619.

20. Hanema, J.; Lazar, M.; Tóth, R. Tube-based LPV constant output reference tracking MPC with error bound. *IFAC-PapersOnLine* **2017**, *50*, 8612–8617.